ISSN 2224-087X. Електроніка та інформаційні технології. 2023. Випуск 22. С. 3–14
Electronics and information technologies. 2023. Issue 22. P. 3–14

УДК 52.17 DOI: https://doi.org/10.30970/eli.22.1

1-D INTERFEROMETER IN 3-D SPACE AND RADON TRANSFORM

A. Lozynskyy, B. Rusyn, O. Ivantyshyn

Karpenko Physico-Mechanical Institute of the National Academy of Sciences of Ukraine,
5, Naukova str.,Lviv, 79060, Ukraine
lozynskyy.a@gmail.com

Observations in three-dimensional space using an interferometer generally require a corresponding rank of the base vector system of the interferometric system. The paper considers one of the ways to solve such a problem using a 1D interferometer with a moving antenna. Due to its movement, it is possible to synthesize an interferometer of a higher rank, similar to aperture synthesis. Moving the moving antenna in the plane allows formation of a 2D interferometer. The obtained analytical expressions show that such an interferometer performs the Radon transform of the angular structure of the spatial image when observing sources far beyond the size of the interferometer base. In the quasi-monochromatic approximation, a comparison is made between the van Cittert-Zernike theorem, which is widely used in such problems, and the considered transformation. It is shown that the obtained conclusions agree well with each other, while the Radon transform better meets the problem and is free from a number of limitations.

Key words: 1D and 2D interferometers, aperture synthesis, Radon transform, mutual coherence function, angular intensity distribution.

Introduction.

1D interferometry is widely used in various scientific and technical studies. In high-precision mirror metrology, the stitching of surfaces based on accurate measurement of angles is successfully used [1]. In seismology – for monitoring the state of building structures during earthquakes using the interferometric method [2], for evaluating the S-wave velocity model in mining regions characterized by strong seismicity [3]. In non-destructive testing of materials – for reliable and sensitive detection of ultrasound [4]. In addition, there are applications of 2D interferometers in which phase coding is carried out along the second dimension [5] and 3D interferometers based on interferometry of real thermal light intensities [6] and three-dimensional stochastic interferometry [7].

The technology of aperture synthesis, which is based on the application of the van Cittert-Zernike theorem [8], has become particularly widely used in radio astronomy. It boils down to the joint processing of data obtained by many two-element interferometers. The antenna system is divided into pairs. Based on the transverse correlation function obtained for each pair, the value of the corresponding spatial harmonic of the Fourier transform of the image is founding [9]. To correctly solve the inverse problem - image restoration - it would be necessary to have an infinite number of such harmonics, but this is impossible in principle. Therefore, various methods of interpolation and processing of incomplete data are used, for example, compressed sounding and sparse restoration [10]. The resolution and quality of the reconstruction results significantly depends on the set of baselines of the antenna system and the applied methods. The implementation of such a technology requires the satisfaction of a number of approximation

conditions, including: the plane wave approximation, the delta-correlation approximation of the source points, the approximation of the object field of view to the plane and the limitation of its dimensions, the quasi-monochromatic approximation, the approximation of the homogeneity of the wave propagation medium, the approximation of the completeness of filling the area of interferometric bases. Some of these approximations are rather difficult to ensure, and a number of methods are being developed to reduce the impact of their violation, including undersampling and deconvolution, isoplanatism [11], spectral behavior [12], non-coplanarity [13], direction-dependent calibration effects [14], etc. The difficulties of taking into account the inhomogeneities of the medium of wave propagation, primarily the non-stationary ionosphere, give rise to the so-called phase problem in low-frequency radio astronomy [15, 16]. In addition, reconstruction of radio images belongs to the class of inverse incorrect problems. Therefore, the search for new stable algorithms for its solution is still relevant today. At the same time, despite all the associated problems, interferometers that are functioning today and new ones that are being built or designed are systems of aperture synthesis.

Another known approach is based on the use of the longitudinal correlation function [17] followed by the Radon transform [18]. The antenna system is similarly divided into pairs, a set of projections is obtained and the inverse Radon transform is performed. With such a reconstruction technology, the quasi-monochromatic approximation becomes unnecessary, the resistance to the influence of the inhomogeneity of the propagation medium increases, and the filling of the area of the interferometric bases is improved. But at the same time, a strict solution is still achieved only with an infinite number of projections, which again requires the use of interpolation procedures.

A fundamentally different view of the problem of image reconstruction is considered in [19], in which the inverse problem of image reconstruction is posed correctly. In it, conclusions were drawn about the bijection of the transformation of spatial and differential coordinates and that presenting the problem in differential coordinates allows one to move from hyperbolic localization of image elements to localization in the Cartesian coordinate system, in which is much more convenient to operate.

Two-element (1D) interferometer.

Let the interferometer be formed by two antennas (sensors), the first of which (A) is placed at the origin of coordinates, and the second (A_1) sets the radius vector of the interferometric base $\boldsymbol{d} = \overrightarrow{AA_1}$. By $\boldsymbol{r}_1$ we denote the vector from the location point of the antenna A_1 to the point in space specified by the radius vector $\boldsymbol{r}$. Then:

$$\boldsymbol{d} + \boldsymbol{r}_1 = \boldsymbol{r}. \tag{1}$$

The difference in distances from a point in space to the antennas of the interferometer l is written in the form

$$l = r - r_1. \tag{2}$$

Taking (1) into account, expression (2) will take the form

$$l = r - \sqrt{r^2 + d^2 - 2\boldsymbol{r}\boldsymbol{d}}, \tag{3}$$

or, after squaring

$$l^2 - 2rl = r - d^2 - 2\boldsymbol{rd}\,. \tag{4}$$

Note that $-d \le l \le d$.

Let the function $f(\boldsymbol{r})$ be defined in the entire space and decay quickly enough to infinity (so that the corresponding improper integrals converge). Then the transformation carried out by the interferometer can be conveniently expressed using the Dirac delta function

$$G(l,\boldsymbol{d}) = \int \delta\left(r - \sqrt{r^2 + d^2 - 2\boldsymbol{rd}} - l\right) f(\boldsymbol{r})\,d\boldsymbol{r}\,. \tag{5}$$

The integration here is carried out over the entire space, $d\boldsymbol{r} = dxdydz$.

As shown in [19], in this form, the two-element interferometer is suitable for solving problems of object localization in 1D space, and in higher dimensional spaces, the solution of equation (3) is multivalued. This is a hyperbola in the case of 2D space and a two-cavity hyperboloid in 3D space, along which the integration in (5) takes place.

As an option, [19] considers the synthesis of a higher-rank interferometer (that is, an interferometer whose bases vectors system has a higher rank) based on several 1D interferometers. Under the condition of quasi-stationarity of the analyzed spatial scene, only one but with a moving antenna A_1, can be used as several interferometers, which allows to obtain information for different vectors of the interferometric base in a sequence.

In the general case, the law of motion of the base vector of the interferometer can be quite complex to ensure certain qualities of the system, but we will stop at a common method known as aperture synthesis. In this case, the interferometric base vector $\boldsymbol{d}$ rotates in the plane, providing, under certain approximations, a 3D scene analysis.

1D interferometer and Radon transform.

To simplify the calculations, let the vector $\boldsymbol{d}$ of constant length rotate uniformly in the xOy plane with an angular frequency ω such that changes in the 3D scene can be neglected during one revolution. Then you can write in the coordinate form

$$\boldsymbol{d}(t) = (d\cos\omega t, d\sin\omega t, 0). \tag{6}$$

Let us assume that $f(\boldsymbol{r})$ is equal to zero everywhere, with the exception of one point S, whose radius vector is $\boldsymbol{r}_s$. In spherical coordinates (r,θ,φ), expression (3) for the point S will have the form

$$l_s(\varphi) = r_s - \sqrt{r_s^2 + d^2 - 2r_s d\sin\theta_s\cos\varphi}\,, \tag{7}$$

where $\varphi = \omega t - \varphi_s$.

Let's analyze the appearance of the trace $l_s(\varphi)$ of the point S on the image of the transformation G at different values of r_s. It is clear from equation (3) that l reaches extremes when the projection of the vector $\boldsymbol{r}_s$ on the plane xOy coincides with the direction of the vector $\boldsymbol{d}$, or is opposite to it. In Fig. 1a shows a family of curves obtained for different r_s. For clarity, $d = 1$ is set, and θ_s are chosen so that at $\varphi = 0$ the values of l for different r_s coincide. Note

that as r_s increases, the curves begin to resemble a sinusoid (solid lines). To explain this, let's divide the right and left parts of expression (4) by r and consider it for the approximation $r >> d$ (similar to the plane wave approximation $r \to \infty$, which is often used in interferometry, but somewhat weaker). Then the terms $\frac{l^2}{r}$ and $\frac{d^2}{r}$ can be neglected due to their smallness. Expressions (4) and (7) then take the form

$$l = \frac{\boldsymbol{r}}{r}\boldsymbol{d}\,, \tag{8}$$

its solution is a cone asymptotic to the hyperboloid given by equation (4) and

$$l_s(\varphi) = \frac{\boldsymbol{r}_s}{r_s}\boldsymbol{d}\sin\theta_s\cos\varphi\,. \tag{9}$$

It can be seen from here that at large distances from the point, its trace becomes sinusoidal with an amplitude that depends on the coordinate θ_s and a phase determined by the coordinate φ_s.

In Fig. 1b shows a picture of a group of traces for several different points, the distance of which from the origin of coordinates significantly exceeds the length of the interferometer base (obtained at $d = 1$). Its similarity with the Radon sinogram is clearly obvious.

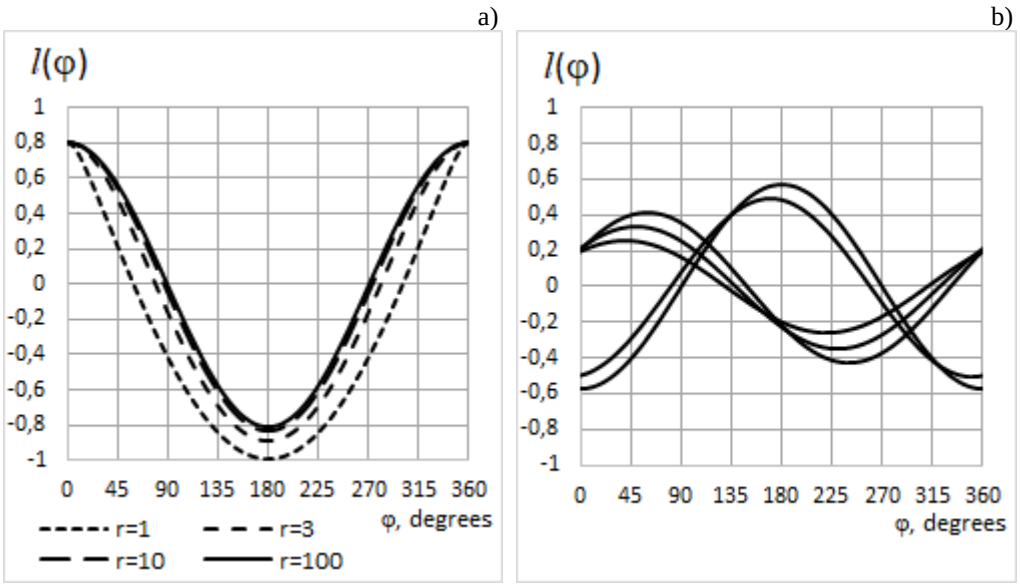

Fig. 1. View of the traces $l(\varphi)$ on the image of the transformation G: a) for several points with different values of r_s at initial value of $l = 0.8$; b) for two groups of points at $r_s = 100$

To explain this, consider how equation (5) changes in $r >> d$ approximation. If we divide equation (8) by d and enter the notation of the relative difference coordinate $\eta = \frac{l}{d}$ and the unit vector in the direction of the interferometric base vector $\boldsymbol{n} = \frac{\boldsymbol{d}}{d}$, then:

$$\eta = \boldsymbol{n}\frac{\boldsymbol{r}}{r}. \tag{10}$$

Equation (5) can then be rewritten as follows

$$G(\eta, \boldsymbol{n}) = \int \delta\left(\boldsymbol{n}\frac{\boldsymbol{r}}{r} - \eta\right) f(\boldsymbol{r}) d\boldsymbol{r}. \tag{11}$$

Integration here, as in (5), is also carried out over the entire space. The transformation $G(\eta, \boldsymbol{n})$ is the integral of the function $f(\boldsymbol{r})$ in the entire space over a cone with the angle at the apex depending on η and the axis oriented in the direction $\boldsymbol{n}$. Let us now define the function $\hat{f}(\boldsymbol{r})$, which is equal to zero in all space except for the sphere of unit radius centered at the origin, and its value is the central projection of the function $f(\boldsymbol{r})$ onto this sphere. In this case, the argument of the Dirac function in (11) can be expanded to $\boldsymbol{nr} - \eta$ without changing the value of the integrand. As a result, we get:

$$G(\eta, \boldsymbol{n}) = \int \delta(\boldsymbol{nr} - \eta) \hat{f}(\boldsymbol{r}) d\boldsymbol{r}. \tag{12}$$

As it is easy to see the form of the obtained expression fully coincides with the definition of the multidimensional Radon transform, for which a number of methods of solving the inverse problem are known [20].

Thus, the transformation performed by the 1D interferometer when implementing all possible interferometric bases $\boldsymbol{d}$ in space is the Radon transform of the function $\hat{f}(\boldsymbol{r})$ – the central projection onto the sphere of the original function $f(\boldsymbol{r})$ supplemented with zeros. The latter is defined in the entire space, but is different from zero only at $r >> d$, that is, in the far part of the space.

Note that the function $\hat{f}(\boldsymbol{r})$ actually depends only on the angular coordinates and its addition with zeros was necessary only to establish the general form of the transformation performed by the 1D interferometer and its connection with the Radon transform.

But let's return to the above-described version of the interferometer with antenna A_1, which rotates around antenna A in the xOy plane. It is easy to show that since the z component of the vector $\boldsymbol{d}$ is zero, the scalar product $\boldsymbol{n}\frac{\boldsymbol{r}}{r} = \sin\theta\cos(\psi - \varphi)$, where $\psi = \omega t$. Equation (11) will then take the form

$$G(\eta, \psi) = \iint \delta(\sin\theta\cos(\psi - \varphi) - \eta) f(\theta, \varphi) \sin\theta d\theta d\varphi, \tag{13}$$

which, as is easy to see, is a two-dimensional Radon transform.

We can conditionally say that equations (12) and (13) correspond to three sequential projections (Fig. 3). First, the central projection is carried out onto the unit sphere of the part of space for which $r >> d$. Then the sphere is projected onto the xOy plane. Finally, the point with coordinates $(\sin\theta, \varphi)$ is projected onto the vector $\boldsymbol{n}$ to a point p, from which relative difference coordinate $\eta = 2p - 1$ is determined.

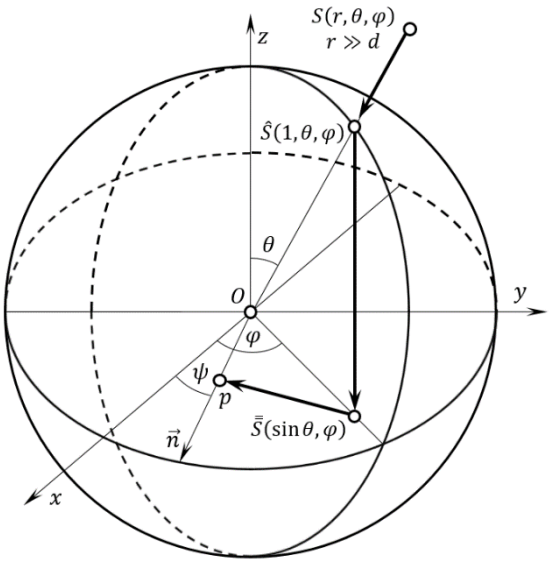

Fig. 2. Illustration of the sequence (bold lines) of projecting an element of space $S(r, \theta, \varphi)$:

1) $\hat{S}(1, \theta, \varphi)$ – the central projection on the unit sphere;
2) $\bar{\bar{S}}(\sin\theta, \varphi)$ – the projection of the sphere onto the xOy plane;
3) p – the projection of the point $\bar{\bar{S}}(\sin\theta, \varphi)$ onto the vector $\boldsymbol{n}$, $p = (\eta - 1)/2$

It is important to note that the operation of projecting the sphere onto the xOy plane leads to ambiguity – two points (on the upper and lower hemispheres) are projected into one. The solution to this problem is possible, for example, when using directional antennas or under the condition of such a movement of the antenna A_1, in which the vectors of the bases will not lie in the same plane.

Radon transform and the van Cittert-Zernike theorem.

The van Cittert-Zernike theorem considers two very distant parallel planes, both perpendicular to the line of sight, the source plane and the observation plane (Fig. 3). If

$\Gamma_{12}(u,v,0)$ is a function of mutual coherence between two points P_1 and P_2 on the observation plane, then

$$\Gamma_{12}(u,v,0) = \iint I(l,m) e^{-2\pi i(ul+vm)} dldm , \tag{14}$$

where l and m are the directional cosines of the radius vector of a point on a distant source in the source plane $\boldsymbol{r}$, u and v are, respectively, the x-distance and y-distance between observation points in wavelength units, and I is the intensity of the source [8].

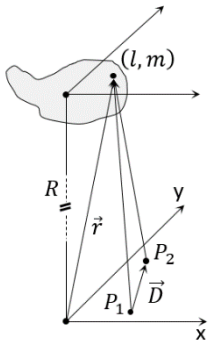

Fig. 3. To the output of the difference in distances from the point (l,m) in the source plane to points P_1 and P_2 in the observation plane

We consider the plane wave approximation, that is, $R \to \infty$. Analogously to conclusion (8), we obtain the differences of the distances L_1 and L_2 from the point with coordinates (l,m) to the origin of the coordinates and to the antenna placement points P_1 and P_2, respectively:

$$\begin{aligned} L_1 &= \frac{\boldsymbol{r}}{r}\boldsymbol{P}_1 \\ L_2 &= \frac{\boldsymbol{r}}{r}\boldsymbol{P}_2 \end{aligned} . \tag{15}$$

Hence, marking the base vector $\boldsymbol{D} = \boldsymbol{P}_2 - \boldsymbol{P}_1$, we will find the difference of distances $L = L_2 - L_1$ to points P_1 and P_2:

$$L = \frac{\boldsymbol{r}}{r}\boldsymbol{D} \tag{16}$$

(note that the uniformity of the form of expressions (8), (15) and (16) illustrates the fact of their independence from the parallel transfer of the base vector of the interferometer in the approach of a plane wave).

If we continue to consider expression (16) as described above, we will arrive at the Radon transform, and otherwise, we will consider it under the quasi-monochromatic approximation.

Then the distance difference determines the difference in wave phases at the observation points with a period equal to the wavelength λ. Dividing the right and left parts of (16) by λ, we get

$$\frac{L}{\lambda} = \frac{\boldsymbol{r}}{r}\frac{\boldsymbol{D}}{\lambda}. \tag{17}$$

The ratio $\frac{\boldsymbol{r}}{r}$ is a unit vector given by direction cosines (l,m), when writing the scalar product in (17) in coordinate form, we get

$$2\pi\frac{L}{\lambda} = 2\pi(ul+vm), \tag{18}$$

which is an index of the complex exponent in the van Cittert-Zernike theorem.

It should be noted that the above-mentioned ambiguity is manifested here as well – measurements in the observation plane do not allow to determine whether the source plane is located above or below it.

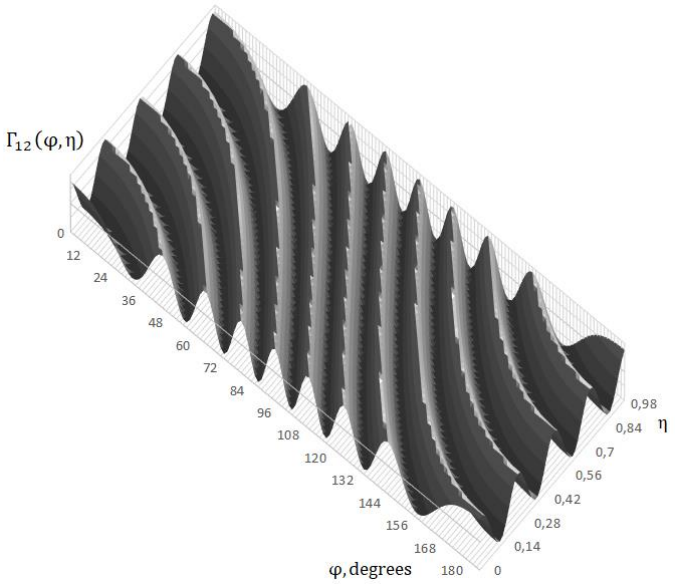

Fig. 4. ¼-fragment of the real part of the mutual coherence function $\Gamma_{12}(u,v,\tau)$, which corresponds to the observation of a point source for half a revolution of the interferometer in the range from $\tau = 0$ to $\tau = \tau_{\max}$ for $u = \cos\varphi$, $v = \sin\varphi$ and $\eta = \frac{\tau}{\tau_{\max}}$, calculated using the quasi-monochromatic approximation at $\frac{D}{\lambda} = 4$

In Fig. 4 shows the ¼-fragment of the real part of the mutual coherence function $\Gamma_{12}(u, v, \tau)$, which corresponds to the observation of a point source for half a revolution of the interferometer in the range from $\tau = 0$ to $\tau = \tau_{max}$ for $u = \cos\varphi$, $v = \sin\varphi$ and $\eta = \frac{\tau}{\tau_{max}}$, calculated using the quasi-monochromatic approximation at $\frac{D}{\lambda} = 4$. The van Cittert-Zernike theorem applies to data that are the cross section of the given function at η, $\tau = 0$ (shown in Fig. 5).

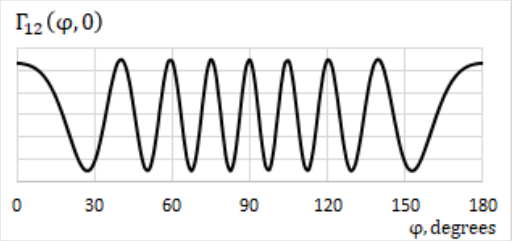

Fig. 5. Section of the real part of the mutual coherence function shown in Fig. 4, when $\eta = 0$

It is clear that the transformation obtained under such conditions can no longer be considered a Radon transform. But, if the set of dependencies calculated for different θ, similar to the one shown in Fig. 5, to be taken as a set of directional diagrams of the antenna-recording system, then it can be considered as a Radon transform in generalized projections when scanning along the φ coordinate [21].

Conclusion.

Observations in three-dimensional space using an interferometer generally require a corresponding rank of the base vector system of the interferometric system. The paper considers one of the ways to solve such a problem using a 1D interferometer with a moving antenna, due to its movement, it is possible to synthesize a higher-rank interferometer, similar to the well-known method of aperture synthesis. Moving the moving antenna in the plane allows you to synthesize a 2D interferometer. The obtained analytical expressions show that such an interferometer performs the Radon transform of the angular structure of the spatial image when observing sources far beyond the size of the interferometer base.

A comparison of the van Cittert-Zernike theorem, which is widely used in such problems, and the considered transformation are made. It is shown that the conclusions obtained under the quasi-monochromatic approximation are consistent with each other, while the Radon transform better meets the problem and is free from a number of limitations. With this approach, the field of view is not limited, the quasi-monochromatic approximation is not required, resistance to the influence of the inhomogeneity of the wave propagation medium is increased, and the filling of the interferometric base area is improved.

It is noted that in both cases (the application of the Radon transform or the van Cittert-Zernike theorem) there is an ambiguity – the solutions are symmetric with respect to the plane defined by the base vectors of the interferometer.

REFERENCES

[1] *Huang L., Janpeng X., Idir M.* One-dimensional angular-measurement-based stitching interferometry // Optics Express. - 2018. - Vol. 26, No. 8. P. 9882-9892. https://doi.org/10.1364/OE.26.009882

[2] *Rahmani M, Todovska M.* 1-D system identification of buildings during earthquakes by seismic interferometry with waveform inversion of impulse responses-method and application to Millikan library // Soil Dynamics and Earthquake Engineering. - 2013 - Vol. 47. P. 157-174. https://doi.org/10.1016/j.soildyn.2012.09.014

[3] *Czarny R, Pilecki Z., Drzewińska D.* The application of seismic interferometry for estimating a 1-D S-wave velosity model with the use of mining induced seismicity // Journal of Sustainable Mining. - 2018. - Vol. 17, No. 4. P. 209-214. https://doi.org/10.1016/j.jsm.2018.09.001

[4] *Blum T., Ponet B.,Breugnot S.,Clemenceau P.* Non-destructive testing using multi-channel random-quadrature interferometer. AIP conference proceeding, 975.299, - 2008. - https://doi.org/10.1063/1.2902664

[5] *Birge J., Ell,R., Kartner F.* Two-dimensional spectral shearing interferometry for few-cycle pulse characterization // Optics Letters. - 2006. - Vol. 31, No. 13. P. 2063-2065. https://doi.org/10.1364/OL.31.002063

[6] *Wagner F., Schiffers F., Willomitzer F., Cossairt O., Velten A.* Intensity interferometry-based 3D imaging // Optics Express. - 2021. - Vol. 29, No. 4. P. 4733-4745. https://doi.org/10.1364/OE.412688

[7] *Graciani G., Filoche M., Amblard F.* 3D stochastic interferometer defects picometer deformations and minute dielectric fluctuations of its optical volume // Communications Physics. - 2022. - Vol. 5, No. 239. https://doi.org/10.1038/s42005-022-01016-9

[8] *Thompson A. R.* Interferometry and Synthesis in Radio Astronomy / A. Richard Thompson, James M. Moran, George W. Swenson, Jr.; 3rd ed. Springer, 2017. http://doi.org/10.1007/978-3-319-44431-4

[9] *Scaife A. M. M.* Big telescope, big data: towards exascale with the Square Kilometre Array // Phil. Trans. R. Soc. – 2019 – id. A.3782019006020190060. https://doi.org/10.1098/rsta.2019.0060

[10] *H. Garsden, J. N. Girard, J. L. Starck et al. (78 more)*. LOFAR sparse image reconstruction // A&A. - 2015 – Vol. 575, id. A90, 18 pp. https://doi.org/10.1051/0004-6361/201424504

[11] *Schwab F. R.* Relaxing the isoplanatism assumption in self-calibration; applications to low-frequency radio interferometry // The Astronomical Journal. - 1984. - Vol. 89. P. 1076–1081. http://doi.org/10.1086/113605

[12] *Taylor G., Carilli C., Perley, R.* Synthesis imaging in radio astronomy II // ASP Conference Series. - 1999. - Vol. 180.

[13] *Shopbell P., Britton M., Ebert R.* Astronomical Data Analysis Software and Systems XIV // Astronomical Society of the Pacific Conference Series. - 2005. - Vol. 347.

[14] *Bhatnagar S., Rau U. and Golap, K.* Wide-field wide-band interferometric imaging: the WB a-projection and hybrid algorithms // The Astrophysical Journal. - 2013. - Vol. 770, No. 2, p. 91. https://doi.org/10.1088/0004-637X/770/2/91

[15] *Kornienko Yu. V., Skuratovskiy S. I.* On the image reconstruction under its Fourier-transform modulus // Radiofiz. elektron. - 2008. - Vol. 13, No. 1, P. 130-141.

[16] *Kornienko Y., Lyashenko I., Pugach V., Skuratovskiy S.* Accumulation of Fourier Component Phases during Observation of an Object with an Orbital Telescope // Kinematics and Physics of Celestial Bodies. - 2020. - Vol. 36, No. 1, P. 37-45.
[17] *Koshovy V. V., Lozynsky A. B.* The radio image restoring of space radio sources based on the longitudinal cross-correlation function // Information extraction and processing. - 1998. - Vol. 12 (88), PP. 37-41.
[18] *Koshovyy V.; Lozynskyy A.; Lozynskyy B.* The tomographic technique for reconstruction of the cosmic radio sources images on the basis of radio interferometric data // XXVIIth General Assembly of the International Union of Radio Science. - 2002. https://doi.org/10.5281/zenodo.7950758
[19] *Lozynskyy A., Ivantyshyn O., Rusyn B.* Using multi-position interferometry to determine the position of objects // Information and Communication Technologies, Electronic Engineering. - 2022. - Vol. 2, No. 1, P.52-60. https://doi.org/10.23939/ictee2022.01.052.
[20] *Natterer, F.* The Mathematics of Computerized Tomography. John Wiley & Sons. New York - 1986. - 240p.
[21] *Lozynsky A., Romanyshyn I., Rusyn B.* Tomographic Image Reconstruction Based on Generalized Projections // Cybernetics and System Analysis. - 2021. - Vol. 57, No. 3, P. 463-469. https://doi.org/10.1007/s10559-021-00371-9

1-D ІНТЕРФЕРОМЕТР В ТРИВИМІРНОМУ ПРОСТОРІ І ПЕРЕТВОРЕННЯ РАДОНА

А. Лозинський, Б. Русин, О. Івантишин

Фізико-механічний інститут ім. Г.В. Карпенка НАН України,
вул. Наукова, 5, 79060, м. Львів, Україна
lozynskyy.a@gmail.com

Спостереження в тривимірному просторі з допомогою інтерферометра в загальному випадку вимагають відповідного рангу системи векторів баз інтерферометричної системи. В радіоастрономії особливо широкого застосування набула технологія апертурного синтезу, яка опирається на застосування теореми ван Цітерта-Церніке. Вона зводиться до сумісного обробітку даних, отриманих багатьма двоелементними радіоінтерферометрами. На основі отриманої для кожної пари антен поперечної кореляційної функції знаходиться значення відповідної просторової гармоніки Фур'є-перетворення зображення. Результат отримується зворотним Фур'є-перетворенням. Реалізація такої технології вимагає задоволення умов ряду наближень, причому деякі з них досить проблематичні, до прикладу – вимоги до однорідності середовища поширення хвиль.

В роботі розглянуто один з альтернативних шляхів вирішення такої задачі за допомогою 1D інтерферометра з рухомою антеною, за рахунок переміщення якої, подібно як і при апертурному синтезі, синтезується інтерферометр вищого рангу. При цьому реєструється поздовжня кореляційна функція сигналів, прийнятих антенами радіотелескопа. Переміщення рухомої антени в площині дозволяє утворити 2D інтерферометр і виконати спостереження проєкції простору на цю площину. Отримані аналітичні вирази показують, що такий інтерферометр здійснює перетворення Радона кутової структури просторового зображення при спостереженні джерел, віддалі до яких значно перевищують величину бази інтерферометра.

Проведено порівняння за квазімонохроматичного наближення широко застосовуваної в таких задачах теореми ван Цітерта-Церніке і розглянутого перетворення. Показано, що отримані висновки добре узгоджуються між собою, при цьому перетворення Радона краще відповідає задачі і вільне від ряду обмежень. Зокрема при такому підході не обмежується поле зору, не вимагається наближення квазімонохроматичності, підвищується стійкість до впливу неоднорідності середовища поширення хвиль і покращується заповнення області інтерферометричних баз. Тому його реалізація є перспективною для впровадження в різних застосуваннях.

Ключові слова: 1D та 2D інтерферометри, апертурний синтез, перетворення Радона, функція взаємної когерентності, кутовий розподіл яскравості.

Стаття надійшла до редакції 19.06.2023.
Прийнята до друку 24.06.2023.